,661 2SHQ $FFH

šÞ-¥Ä$ ^ûÄåªšÞ-Þ ‚Ä– Äå-=WÚË½- < 0 /Äª-•-åËÚû ‚Ä– DË½š•é½‚Ú Ë šÚå‚-Ä Ešõ ^é•Þå-åéåš– WûÚ-Ã-––Ä

$O 5DVKRRG 6DUDL7$PDO 6 DQG $ONDKWDQL +DPDG 0

'HSDUWPHQW RI 3KDUPDFHXWLFDO &KHPLVWU\ &ROOHJH RI 3KDUPDF\ .LQJ 6DXG 8QLY

$EVWUDFW

1RYHO VHULHV RI S\ULPLGLQH GHULYDWLYHV D R ZHUH V\QWKHVL]H FRORUHFWDO &7 FDUFLQRPD FDUFLQRPD +H/D DQG EUHDVW FDUFLQRPD DFWLYH RQHV DJDLQVW +&7 +H/D DQG &ROR OLQHV UHVSHFWLYHO\ WR GR[RUXELFLQ ,& 'Ø UHVSHFWLYHO\ &HOO F\FOH DQDO\VLV WUHDWPHQW RI +&7 +H/D FHOOV ZLWK FRPSRXQGV XS DQG GRZQ UHJXODWLRQ $SRSWRWLF HIIHFW RI FRPSRXQGV E DQG D ZHUH HYDOXDWHG GLVSOD\HG SURPLVLQJ &'. DQG &'. LQKLELWRU\ DFWLYLW\ VWXG\ VKRZHG VLPLODU ELQGLQJ PRGHV RI WKH VWXGLHG FRPSRXQGV &'. LVRIRUP 7KHVH ILQGLQJV UHFRJQL]HG FRPSRXQG K DV SRWHQW &'. LQKLELWLRQ DFWLYLW\

.H\ZRUGV 3\ULPLGLQHV • $QWLSUROLIHUDWLYH • $SRSWRVLV • &'. • &'. • 0RO

,QWURGXFWLRQ

&DQFHU UHSUHVHQWV RQH RI WKH OHDGLQJ FDXVHV RI GHDWK ZRUOGZLGH ,UUHVSHFWLYH RI WKH SURJUHVVHV JRWWHQ LQ FDQFHU WUHDWPHQWV OLPLWDWLRQV VWLOO SUHVHQW DV FDQFHU FHOOV HYHQWXDOO\ EHFRPH UHVLVWDQW WR WKH PXOWLSOH GUXJ UHJLPHQ $FFRUGLQJO\ LQYHQWLRQ RI QHZ PROHFXOHV ZLWK QRYHO PHFKDQLVPV UHPDLQ FKDOOHQJH ,QFUHDVLQJ DSRSWRVLV JHQHUDWLQJ WKH SURJUDPPHG FHOO GHDWK F\FOH DUH FRQVLGHUHG DPRQJVW 'HSHQGHQW .LQDVHV &'.V DUH UHJXODWRUV &'.V DUH DFWLYDWHG E\ F\FOLQV RFFXUV FDWDO\]LQJ WKH $GHQRVLQH 7ULSKRVSKDWH $73 WUDQVIHU SURWHLQ VXEVWUDWHV 7KH SKRVSKRU\ODWLRQ PDQ\ RI FHOOXODU IXQFWLRQV IRU WKH FHOO JURZWK DQG GLYLVLRQ EHHQ UHODWHG WR WKH KXPDQ FDQFHU 'HSHQGHQW .LQDVH &'. 6LJQLILFDQW DFWLYH LQ YDULRXV WUDQVLWLRQ SKDVH &\FOLQ 'HSHQGHQW .LQDVH &'. SDUWQHU IRU LQFUHDVLQJ FHOO SUROLIHUDWLRQ

WKURXJK WKH 51$ SRO\PHUDVH ,, SKR RI &'. DQG &'. DFWLYLW\ FRXOG RI FDQFHU WUHDWPHQW

/LWHUDWXUH 5HYLHZ

colorectal carcinoma and Ewing's sarcoma mouse xenograft cancer models [22]. Also, CYC-116 (IV) is a derivative of 2-anilinopyrimidine that exhibited inhibition activities against CDK2 and CDK9 (IC_{50}=0.39 and 0.48 μM, respectively), and cytotoxic activity towards MCF7, Hela and HCT-116 (IC_{50}=0.599, 0.590 and 0.340 μM, respectively)(Figure 1) [23]. Moreover, the pyrazolo [1,5-a] pyrimidine analog 4K (BS-194) (V) exposed CDK2 and CDK9 inhibition activities (IC_{50}=3 and 90 nM, respectively) together with its cytotoxic activity towards MCF7 and HCT-116 (IC_{50}=0.3 and 0.1 μM, respectively) [24]. Besides, Dinaciclib (VI) which displayed promising CDK2 and CDK9 inhibitory activities (IC_{50}=1.0 and 4.0 nM) [25,26], has been assessed for various indications of cancer in clinical trials [27].

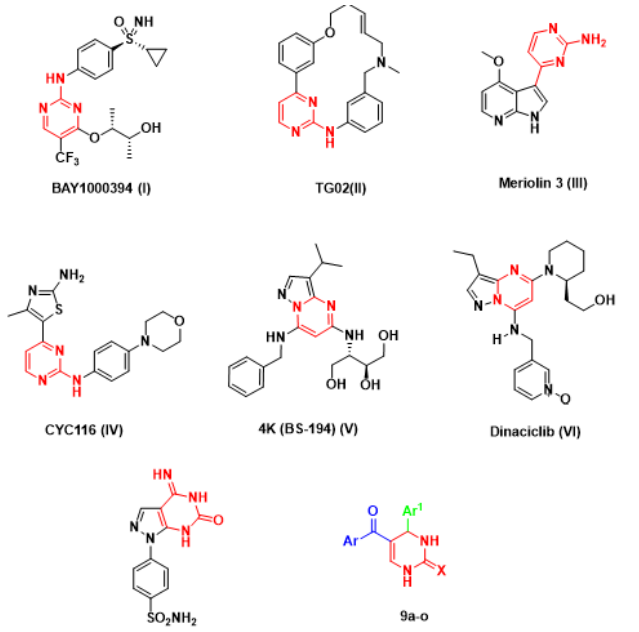

Figure 1. Structures of some lead antitumor pyrimidine derivatives with reported CDK2 and CDK9 inhibitors I-VII and core structure of the designed pyrimidine analogs 9a-o.

The pyrimidinone derivative VII revealed antitumor activity towards MCF7 cell line (IC_{50}=1.4 μM), CDK2 inhibitory activity (IC_{50}=0.19 μM), together with apoptosis induction and S and G_2/M phases cell cycle arrest [28].

Inspired by these previous findings, our design strategy aimed at the synthesis and investigation of some novel pyrimidine derivatives as potential antitumor agents with expected CDK2 and CDK9 inhibition activity. The core structure of the designed pyrimidine analogs is illustrated in (Figure 1). The anticipated compounds will be screened for their growth inhibitory activity against human colorectal carcinoma HCT-116, cervical carcinoma HeLa and breast carcinoma MCF-7 cell lines, in addition to the CDK2 and CDK9 inhibitory activity. The uppermost active compounds will be investigated for cell cycle analysis, and apoptotic assay. A molecular docking study into CDK2 and also CDK9 was scheduled to gain insight into the possible binding modes of the investigated compounds. Finally, ADMET computational study will be considered to predict the pharmacokinetic and toxicity aspects for the studied compounds (Figure 2).

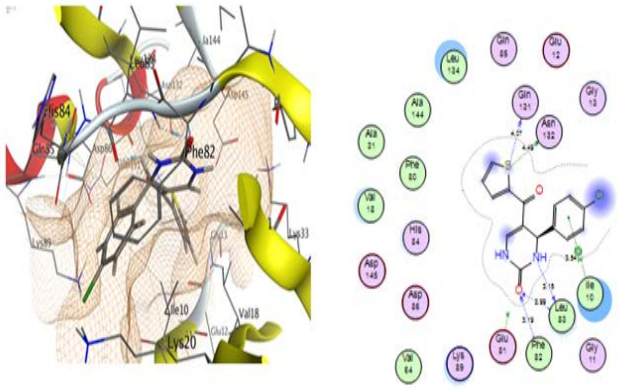

Figure 2: Graphical representation.

(9h)

IC_{50}/MCF-7=3.83 ± 0.27 μM

IC_{50}/CDK2=0.299 ± 0.02 μM

MCF7 cell cycle arrest at G_2/M phase Apoptosis induction

Highlights

Novel pyrimidines were screened for their antiproliferative activity.

Compound 9b, 9k, and 9h inhibits HCT-116, HeLa and MCF-7 growth; (IC_{50}=2.46 ± 0.21, 1.81±0.11 and 3.83 ± 0.27 μM, respectively).

9b, 9k and 9h induce apoptosis and cell cycle arrest at G_1/S and G_2/M phases.

9h and 9e are potent inhibitors for CDK2 and CDK9; (IC_{50} values; 0.299 ± 0.02 and 0.396 ± 0.02, respectively).

Molecular docking revealed comparable binding mode to that of the native ligands.

Results and Discussion

Chemistry

The key starting material enaminones 3a-e are prepared by the reaction of methyl aryl ketones 1a-e with dimethylformamide-dimethylacetal (2) in refluxing xylene [29-30]. Next, three-component cyclocondensation reaction of enaminones 3a-e with with aldehydes 4a-c and urea/thiourea (5a, b) in refluxing acetic acid resulted in the formation of 5-aroyl-4-aryl1-3,4-dihydropyrimidin-2(1H)-one 9a-i and 5-aroyl-4-aryl1-2-thioxo-1,2,3,4-tetrahydropyrimidine9j-o, respectively. This Biginelli-like reaction [31-34] was assumed to proceed through an initial condensation reaction of aldehydes 5a-c with urea/thiourea 5a, b to form the intermediates 6a-f followed by the addition reaction to the double bond in enaminones 3a-e to give intermediate 8a-o which cyclized by the elimination of dimethylamine to afford the pyrimidines 9a-o as final isolable products. The 1H NMR spectra of 9a-o revealed the up-field signal of pyrimidine H-4 around δ 5.50. The D2O exchangeable signals of NH protons in positions 1 and 3 of pyrimidine moiety appeared in the region δ 7.30-10.73. The 13C NMR

spectra of 3,4-dihydropyrimidin-2(1H)-ones 9a-i and 2- thioxo-1,2,3,4-tetrahydropyrimidines 9j-o showed the signal of pyrimidine C-4 in the region δ 49.58-54.88 and 48.47-53.67, respectively. It also showed the signal of pyrimidine C=O in the region δ 150.87-152.74 and aroyl C=O in the region δ 182.78-194.08 for 9a-i whereas the signals of C=S and C=O of 9j-o appeared in the region δ 177.11-174.34 and 180.39-180.88, respectively. In addition, the mass spectra of 9a-o exhibited, in each case, a peak corresponding to their molecular ions. The IR spectra of 9a-o appeared the presence of the characteristic 2NH absorption bands in the region 3050-3400 cm^{-1} in addition to the absorption bands of 2C=O in the region 1589-1712 cm^{-1} for 9a-i and the absorption bands of C=O and C=S in the region 1588-1651 cm^{-1} for 9j-o.

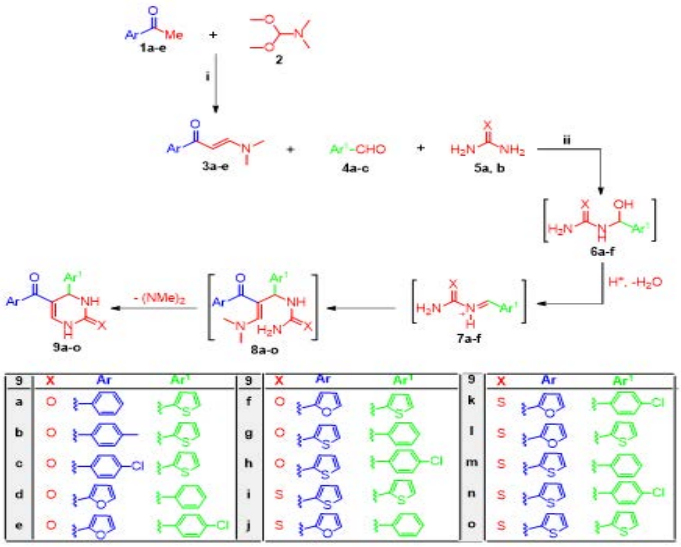

Figure 3. Reagents and conditions: i) dry xylene/reflux 6h; ii) glacial acetic acid/reflux 8 h.

Biological screening

The synthesized pyrimidine derivatives (9a-o) were evaluated for their antiproliferative activity against human colorectal carcinoma HCT-116, cervical carcinoma HeLa and breast carcinoma MCF-7 cell lines. Doxorubicin was used as a control for comparison. The viability of the cells was assessed using the MTT colorimetric assay [35]. The observed growth inhibitory activity of the tested compounds against (9a-o) (Table 1) demonstrates IC_{50} values in micromolar range against HCT-116, HeLa and MCF-7 cell lines Compounds 9b, 9k and 9h were the most active ones against HCT-116, HeLa and MCF-7 cell lines (IC_{50}=2.46 ± 0.21, 1.81 ± 0.11 and 3.83 ± 0.35 μM, respectively) compared to compared to doxorubicin (IC_{50}=2.39 ± 0.16, 3.02 ± 0.18 and 5.56 ± 0.3 μM, respectively). Also, compound 9j is a potent growth inhibitor for Hela cell line with IC_{50} value of 2.15± 0.13 M. Meanwhile, the rest of the tested compounds displayed near to lower growth inhibitory activity against HCT-116, HeLa and MCF-7 cell lines with IC_{50} ranges; 2.87 ± 0.15-182 ± 9.7, 7.52 ± 0.44-96.6 ± 5.64, and 6.5 ± 0.35-153 ± 8.16, respectively in comparison with doxorubicin (Table 1).

Compound	IC_{50} (μM)a		
	HCT-116	HeLa	MCF-7
9a	37.6 ± 2.01	9.32 ± 0.54	24.2 ± 1.29
9b	2.46 ± 0.21	13.8 ± 0.8	13.0 ± 0.69
9c	23 ± 1.23	96.6 ± 5.64	7.2 ± 0.38
9d	84.3 ± 4.5	38 ± 2.22	34.7 ± 1.85
9e	5.62 ± 0.3	7.52 ± 0.44	8.97 ± 0.48
9f	16.7 ± 0.89	19.4 ± 1.13	122 ± 6.51
9g	2.87 ± 0.15	7.78 ± 0.45	26.3 ± 1.41
9h	6.3 ± 0.34	48.6 ± 2.84	3.83 ± 0.27
9i	14.3 ± 0.76	25 ± 1.46	46.6 ± 2.49
9j	6.06 ± 0.32	2.15 ± 0.13	6.5 ± 0.35
9k	182 ± 9.7	1.81 ± 0.11	59.9 ± 3.2
9l	12.6 ± 0.67	10.1 ± 0.59	15.4 ± 0.82
9m	5.28 ± 0.28	33.6 ± 1.96	30.0 ± 1.6
9n	36.7 ± 1.96	14.2 ± 0.83	153 ± 8.16
9o	5.87 ± 0.31	11.1 ± 0.65	32.8 ± 1.75
Dox	2.39 ± 0.16	3.02 ± 0.18	5.56 ± 0.3

Table 1. Growth inhibitory activity (IC_{50} μM) of the tested compounds and doxorubicin against HCT-116, HeLa and MCF-7 cancer cells.

Relating the observed IC_{50} values against HCT-116 cell line of compounds 9a-o to their structural features revealed that the thiophene aryl substitution (-Ar) is more favorable for the growth inhibitory activity than the furan substitution. Illustrative examples are compounds (9g *vs.* 9d: IC_{50} values, 2.87 *vs.* 84.3 µM), (9i *vs.* 9f: IC_{50} values, 14.3 *vs.* 16.7 µM), (9n *vs.* 9k: IC_{50} values, 36.7 *vs.* 182 µM), and (9o *vs.* 9i: IC_{50} values, 5.87 *vs.* 14.3 µM). Additionally, the electronic characteristics of the substituent on Aryl-1 moiety appear to have an influence. Whereby, the electron-withdrawing (Cl) substitution on para position led to reduction in the growth inhibition activity compared to the un-substitution. Examples are compounds (9h *vs.* 9g: IC_{50} values, 6.3 *vs.* 2.87 µM), (9k *vs.* 9j: IC_{50} values, 182 *vs.* 6.06 µM) and (9n *vs.* 9m: IC_{50} values, 36.7 *vs.* 5.82 µM) except compound 9e. For the observed growth inhibitory activity against HeLa cell line, bearing the thioxo side chain group (X=S) attains better growth inhibition activity than the carbonyl group (X=O). This can be exemplified by compounds (9j *vs.* 9d: IC_{50} values, 2.15 *vs.* 38 µM), (9k *vs.* 9e: IC_{50} values, 1.81 *vs.* 7.52 µM), (9l *vs.* 9f: IC_{50} values, 10.1 *vs.* 19.4 µM), (9n *vs.* 9h: IC50 values, 14.2 *vs.* 48.6 µM), and (9o *vs.* 9i: IC_{50} values, 11.1 *vs.* 25 µM), except compound 9g. Moreover, the furan aryl substitution (-Ar) is more preferable here for the growth inhibitory activity than the thiophene substitution; (9e *vs.* 9h: IC_{50} values, 7.52 *vs.* 48.6 µM), (9f *vs.* 9i: IC_{50} values, 19.4 *vs.* 25 µM), (9j *vs.* 9m: IC_{50} values, 2.15 *vs.* 33.6 µM), and (9k *vs.* 9n: IC_{50} values, 1.81 *vs.* 14.2 µM), except for 9d. Also, compounds bearing an electron-withdrawing (Cl) substituent on para position of the Aryl-1 moiety displayed better growth inhibition activity than the un-substituted counterparts, as shown *via* compounds 9e, 9k, 9n *vs.* 9d, 9j, 9m (IC_{50} values; 7.52, 1,81, 14.2 *vs.* 38, 2.15, 33.6 µM, respectively), except for 9h. For the observed growth inhibitory activity against MCF7 cell line, the thioxo side chain group (X=S) is preferable in case of compounds 9j and 9l *vs.* 9d and 9f (IC_{50} values; 6.5 and 15.4 *vs.* 34.7 and 122 µM, respectively). While the carbonyl side chain group (X=O) is desirable in case of compounds 9e and 9h *vs.* 9k and 9n (IC_{50} values; 8.97 and 3.83 *vs.* 59.9 and 153 µM, respectively). Furthermore, the thiophene aryl substitution (-Ar) is more preferable for the growth inhibitory activity in case of compounds 9g, 9h and 9i *vs.* 9d, 9e and 9f (IC_{50} values; 26.3, 3.83 and 46.4 *vs.* 34.7, 8.97 and 122 µM). On the other hand, in case of compounds 9j, 9k and 9l *vs.* 9m, 9n and 9o (IC_{50} values; 6.5, 59.9 and 15.4 *vs.* 30.0, 153 and 32.8 µM, respectively), the furan aryl substitution (-Ar) is more desirable. Also, the electron-withdrawing substituent (Cl) on para position of the Aryl-1 is significant for the growth inhibition activity than the un-substituted counterparts. This could be observed in case of compounds 9e and 9h *vs.* 9d and 9g (IC_{50} values; 8.97 and 3.83 *vs. 34.7 and 26.3*.µM, respectively).

Cell cycle analysis and apoptosis detection

Compounds 9b, 9k and 9h showing the highest anti-proliferative activity against HCT, MCF7 and Hela cell lines, respectively, were chosen for further mechanistic investigation. Their effect on cell cycle progress and apoptosis induction was inspected. Analysis by flow cytometry using BD FASCC alibur was done. This measures the cellular DNA content revealing the cells distribution in the three phases of the cycle and provides an opportunity to found apoptotic cells with fractional DNA content [36]. Cells were treated with the previous compounds at their IC_{50} concentrations, and 48 h incubated. As presented in Table 2 and Figure 3, a high percentage of pre G_1 apoptosis (32.04%) was recorded after treatment of HCT with compound 9b (Control; 1.64%). Besides, a higher cell accumulation (51.31 and 44.19%) was observed at G_0-G_1 and S phases for compound 9b (Control; 46.59 and 42.18%) showing cell cycle arrest at G_1/S phase. Similary, the treatment of Hela cells with compound 9k led to pre G1 apoptotic peak (42.05%) compared to the control; 1.43% (Table 3).

Cells accumulation was also observed at G_0-G_1 and S phases (49.51 and 41.38%), (Control; 46.59 and 42.18%) indicating cell cycle arrest at G_1/S phase for compound 9k. Also, a great percentage of pre G_1 apoptosis (28.04%) was shown after treatment of MCF7 with compound 9h (Control; 2.15%). Moreover, a greater cell accumulation (31.52%) was noticed at the G_2-M phase for compound 9h (Control; 7.52%) indicating cell cycle arrest at G_2-M phase. The results demonstrated that compounds 9b, 9k and 9h inhibit the proliferation of HCT, Hela and MCF7 cell lines, respectively, and cause apoptotic DNA fragmentation (Figures 4 and 5).

Sample	%G_0-G_1	%S	%G_2-M	% pre G_1 apoptosis
HCT Control*	46.59	42.18	11.23	1.64
9b/HCT	51.31	44.19	4.5	32.04
Hela Control	44.51	38.24	17.25	1.43
9k/Hela	49.51	41.38	9.11	42.05
MCF7 Control	53.72	38.76	7.52	2.15
9h/MCF7	43.52	24.96	31.52	28.04

Table 2. Cell cycle analysis after 48 h incubation with the tested compounds.

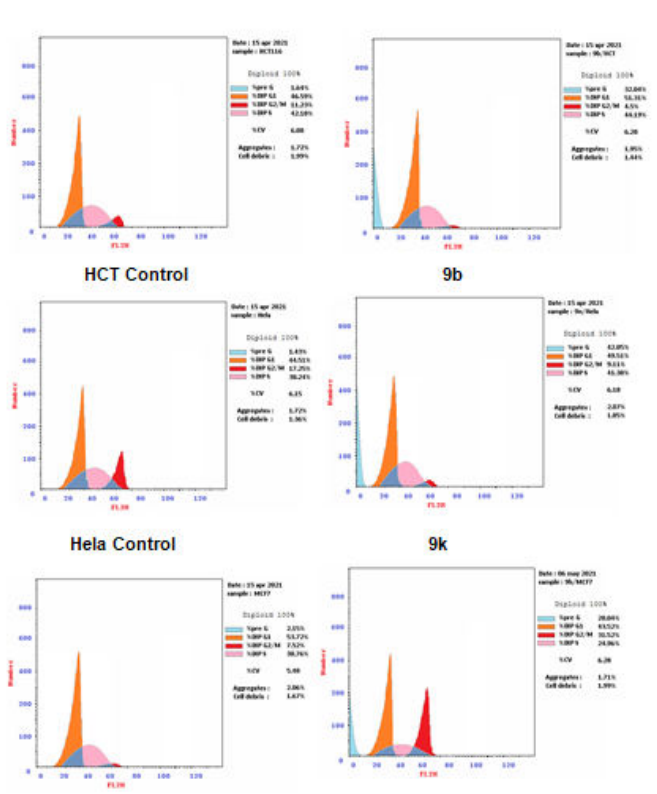

Figure 4. Cell cycle analysis after 48 h incubation with the tested compounds

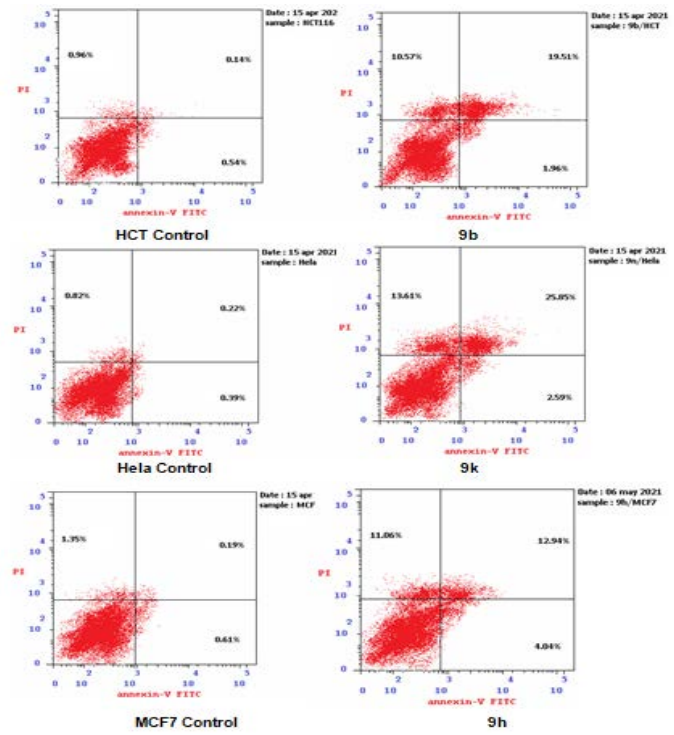

Figure 5. Apoptosis induction analysis after 48 h incubation with the tested compounds.

Apoptosis Assay

Sample	Apoptosis induction analysis		
	Total	Early	Late
HCT Control*	1.64	0.54	0.14
9b/HCT	32.04	1.96	19.51
Hela Control	1.43	0.39	0.22
9k/Hela	42.05	2.59	25.85
MCF7 Control	2.15	0.61	0.19
9h/MCF7	28.04	4.04	12.94

Table 3. Apoptosis induction analysis.

Results of HCT, MCF7 and Hela cells cell cycle analysis after treatment with compounds 9b, 9k and 9h, respectively showed a pre-G_1 peak (Table 2) which is an indication for apoptosis induction. To validate the capability of the tested compounds to induce apoptosis, HCT, MCF7 and Hela cells were stained with Annexin V/PI, incubated for 48 h with 9b, 9k and 9h, respectively, and analyzed. Analysis of early and late apoptosis shows the ability of compounds 9b, 9k and 9h to induce significant levels of apoptosis within the respective treated cells compared to the control cells. The results are summarized in Table 3 and represented graphically in Figure 6.

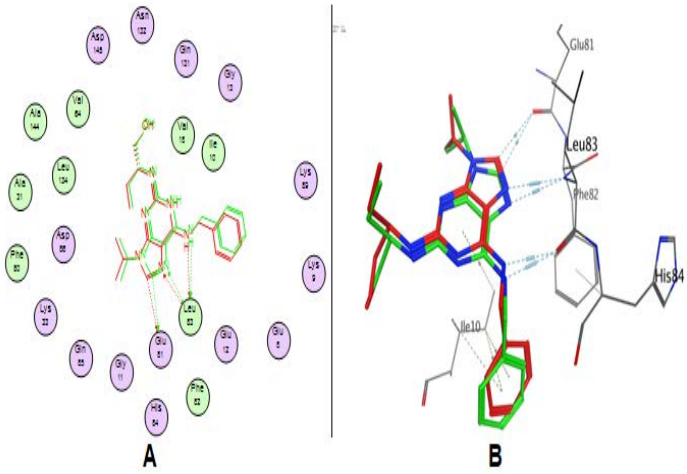

Figure 6. Validation of the used docking protocol; (A) overlay complexes and (B) 3D representation of superimposition of the native ligand (green) and its redocked pose (red) in CDK2 isoform.

Cyclin Dependent Kinase 2/Cycline A2 Enzyme Inhibition

For further mechanistic investigation, all the target compounds 9a-o were assessed for their *in vitro* CDK2/Cycline A2 enzyme inhibition assay. R-Roscovitine has been chosen for comparison as a positive control. The attained dose-response curves were used to calculate IC_{50} values (μM) and are listed in Table 4. Analysis of the CDK2 inhibitory assay results showed that the pyrimidine derivative 9h is the most potent CDK2 inhibitor (IC_{50}: 0.299 ± 0.02 μM) compared to R-Roscovitine (IC_{50}=0.321 ± 0.02 μM). Also, compounds 9b, 9e, and 9m displayed near activity to the reference with IC_{50} values of 0.687± 0.04, 0.392 ± 0.02, 0.62 ± 0.03 μM, respectively. The remaining tested compounds displayed lower inhibitory activity than R-Roscovitine with IC_{50} range (0.993 ± 0.05-20.74 ± 1.09 μM).

Cyclin Dependent Kinase 9/Cycline T_1 Enzyme Inhibition

All the target compounds 9a-o were also assessed for their in vitro CDK9/Cycline T_1 enzyme inhibition assay. R-Roscovitine also has been selected for comparison as a positive control. The attained dose-response curves were used to calculate IC_{50} values (μM) and are listed in Table 4. Results of the CDK9 inhibitory assay results revealed that compound 9e is the most potent CDK9 inhibitor (IC_{50}: 0.396 ± 0.02 μM) compared to R-Roscovitine (IC_{50}=0.456 ± 0.03). Also, compounds 9h, 9m, and 9o displayed near activity to the reference with IC_{50} values of 0.659 ± 0.04, 0.603 ± 0.03, 0.496 ± 0.03 μM, respectively. The remaining tested compounds displayed lower inhibitory activity than R-Roscovitine with IC_{50} range (1.013 ± 0.06-18.52 ± 1.02 μM).

Compound	IC_{50} (μM)a	
	CDK2/CyclinA2	CDK9/CyclinT1
9a	3.654 ± 0.19	5.954 ± 0.33n
9b	0.687 ± 0.04	1.267 ± 0.07
9c	2.899 ± 0.15	1.024 ± 0.06
9d	5.897 ± 0.31	4.733 ± 0.26
9e	0.392 ± 0.02	0.396 ± 0.02
9f	9.803 ± 0.52	17.43 ± 0.96
9g	1.275 ± 0.07	2.837 ± 0.16
9h	0.299 ± 0.02	0.659 ± 0.04
9i	7.071 ± 0.37	5.977 ± 0.33
9j	1.317 ± 0.07	1.013 ± 0.06
9k	13.07 ± 0.69	18.52 ± 1.02
9l	20.74 ± 1.09	7.746 ± 0.43
9m	0.62± 0.03	0.603 ± 0.03
9n	10.33 ± 0.54	3.748 ± 0.21
9o	0.993 ± 0.05	0.496 ± 0.03
R-Roscovitine	0.321 ± 0.02	0.456 ± 0.03

Table 4. CDK2 and CDK9 inhibitory activity (IC_{50} μM) of the tested compounds and R-Roscovitine.

Cyclin Dependent Kinase 9/Cycline T_1 Enzyme Inhibition

All the target compounds 9a-o were also assessed for their in vitro CDK9/Cycline T_1 enzyme inhibition assay. R-Roscovitine also has been selected for comparison as a positive control. The attained dose-response curves were used to calculate IC_{50} values (μM) and are listed in Table 4. Results of the CDK9 inhibitory assay results revealed that compound 9e is the most potent CDK9 inhibitor (IC_{50}: 0.396 ± 0.02 μM) compared to R-Roscovitine (IC_{50}=0.456 ± 0.03). Also, compounds 9h, 9m, and 9o displayed near activity to the reference with IC_{50} values of 0.659 ± 0.04, 0.603 ± 0.03, 0.496 ± 0.03 μM, respectively. The remaining tested compounds displayed lower inhibitory activity than R-Roscovitine with IC_{50} range (1.013 ± 0.06-18.52 ± 1.02 μM).

Molecular modeling study

The obtained CDK2 inhibitory activity exerted by the target compounds and their anti-proliferative activity inspired the examination of the docking pattern into CDK2 enzyme binding site. CDK2 crystal structure co-crystallized with R-Roscovitine was downloaded from PDB and used in the docking investigation. Docking protocol using MOE 2014.0901 molecular modeling program has been applied for this study. A validation step comprising redocking of the native ligand into the binding site is achieved. Validation parameters e.g. RMSD=0.494 A°, and a similar binding mode to that of the native ligand supported the validity of the applied docking protocol (Figure 7). The binding modes revealed that R-Roscovitine fills almost the ATP binding region, where the purine nucleus occupies the adenine area. The interactions show two H bondings among Leu83 amino acid and imidazole core N atom and NH side chain. Moreover, other H-bond was displayed with Glu81 amino acid. The benzyl moiety mediates π-π interaction with the residues; Phe82, Ile10, and His84 [37] (Figure 7).

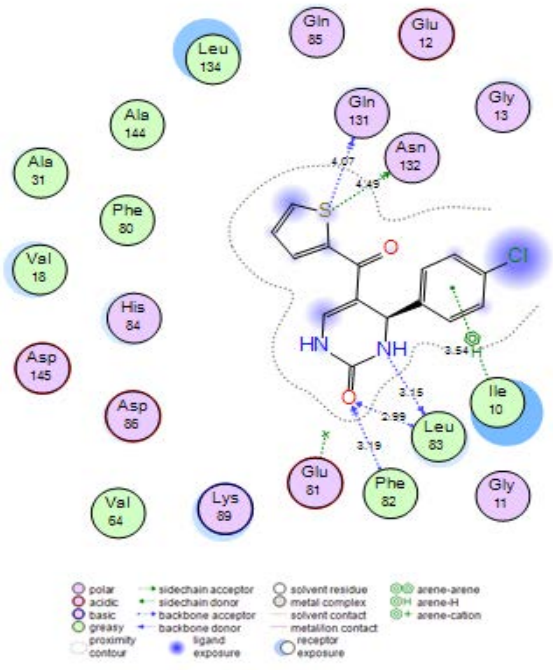

Figure 7. 2D ligand interaction diagram of compound 9h with CDK2 binding site.

Consequently, docking procedures have been completed for the studied compounds. The results demonstrate that most of the studied compounds have similar binding modes with comparable docking scores to that of the lead compound R-Roscovitine. A deep look (Figure 7) on the binding mode of the most potent CDK2 inhibitor 9h (IC50=0.299 ± 0.02 μM) revealed it's binding through two H-bondings to the essential residue Leu83. Also, extra H-bondings to Phe82, Gln131 and Asn132 residues were mediated. Additionally, π-H hydrophobic interaction with Ile10 residue was observed. The binding affinity of compound 9h towards CDK2, represented with its low docking score (S=-11.69 Kcal/mol), as well as its binding mode might rationalize its remarkable CDK2 inhibition activity (Figure 8).

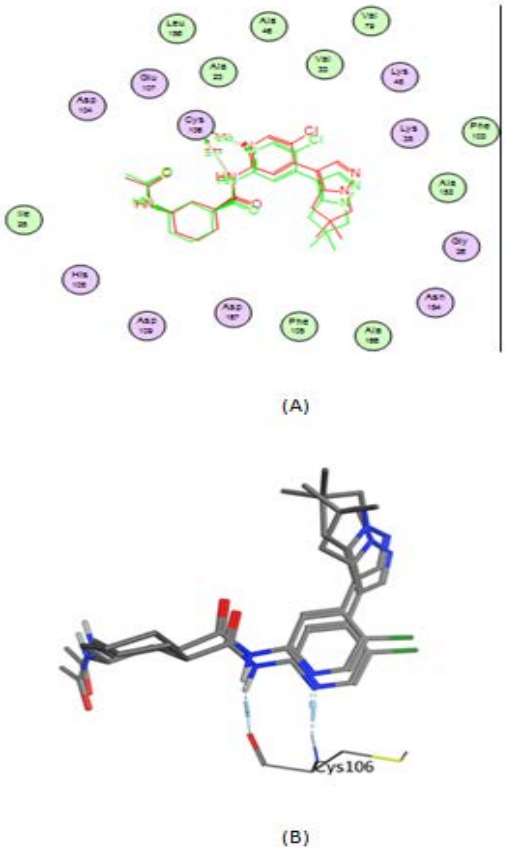

Figure 8. Validation of the adopted docking protocol; (A) overlay complexes and (B) 3D representation of superimposition of the native ligand (green) and its redocked pose (red) into CDK9 isoform.

Molecular Docking into CDK9 Isoform.

Docking study into CDK9 isoform also was performed using MOE 2014.0901 molecular modeling program. structure of CDK9 co-crystallized with the pyridine analogue AZD4573 was downloaded from PDB and used in the docking investigation. Redocking of the native ligand into the binding site was done resulted in RMSD=0.735 A°, together with a similar binding mode to that of the co-crystallized ligand, whereby, AZD4573 binds via two hydrogen-bonds with Cys106 through the pyridyl core N atom and the amidic NH group [38] (Figure 9).

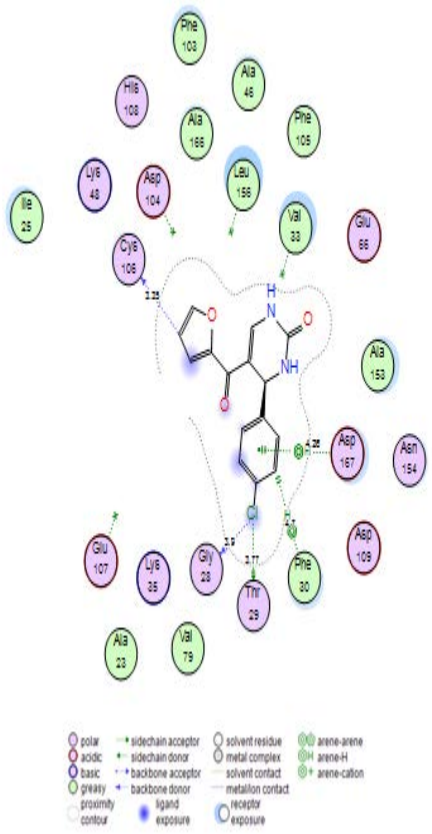

Figure 9. 2D ligand interaction diagram of compound 9e with CDK9 binding site (Docking score "S"=-8.539 Kcal/mol).

The promising CDK9 inhibition activity of compound 9e (IC_{50}=0.396 ± 0.02 μM) might be explained *via* its docking pattern (Figure 10). Whereby, its binding showed H-bonding interaction to the essential Cys106 residue. Additional H-bondings to Gly28, and Thr29 residues were also mediated. Furthermore, π-H hydrophobic interaction with Phe30 and Asp167 residues was observed. The rest of the docked compounds have also comparable binding modes and docking scores to that of the co-crystallized ligand.

In Silicon ADMET Study

Predictions of pharmacokinetics and drug-likeness aspects of the target compounds 9a-o was done using the freely available web server Swiss ADME Human gastrointestinal absorption (HIA), blood-brain barrier (BBB) penetration, substrate or non-substrate for glycoprotein (P-gp) permeability and, interaction of molecules with cytochromes P450 isomers (CYP) werepredicted. Also, bioavailability scores were calculated based on the following five rule-based filters [39], Lipinski [40], Ghose [41], Veber [42], Egan [43] and Muegge [44] rules.

Results of the ADME study are presented as BOILIED-EGG, which is a 2D plot drawn using calculated TPSA and LogP properties of the studied compounds; Figure 10. The white region indicates the GIT passive absorption probability; compounds 9a-d and 9f-o are located in the white area. The yellow region predicts the blood-brain barrier penetration probability; compound 9e is located in the yellow area. Also, all the checked compouds 9a-o might not be substrates for the P-glycoprotein (PGP-), appeared as Red dots, and consequently eliminating the opportunity of its resistance by tumor cell lines through efflux [45], Additionally, most of compounds predicted to show non inhibitory activities on Cytochrome P450 isomers and accordingly are expected to exert no drug-drug interactions upon administration [46] LogKp values which is a interpreter for the skin permeability, the more negative the log Kp (with Kp in cm/s), the less skin permeant is the molecule [47], ranging from -5.95 to -7.09 for the studied compounds. Bioavailability scores were also expected based on compliance of the aimed compounds to Lipinski, Ghose, Veber, Egan and Muegge rules for prediction of their ability to be applied as oral drug candidates. A good oral bioavailability scores were predicted for the compounds; 0.55 (Figures 10, 11 and Tables 5).

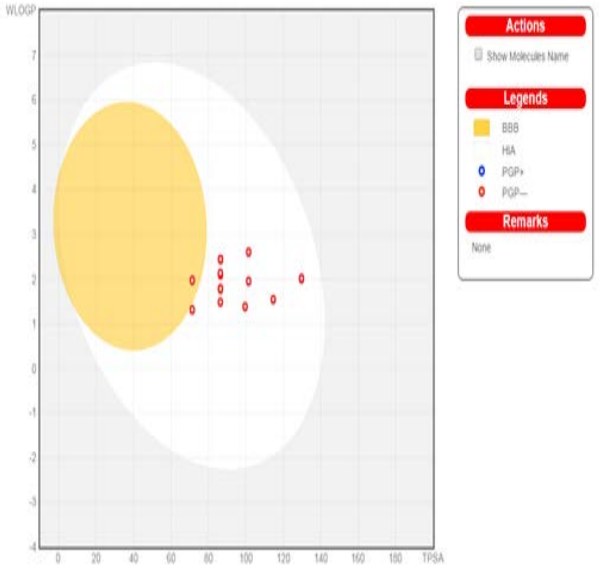

Figure 10. Human intestinal absorption (HIA) and Blood Brain Barrier (BBB) plot for all the studied compounds.

Cpd.	Pharmaco-kinetics					Drug likeness (#violations)						
	GIT Absorption	BBB permeation	Pg-p substrate	CYP2D6	CYP3A4	Logkp skin permeation (cm/s)	Lipiniski	Ghose	Veber	Egan	Muegge	Bioavailability score
9a	High	No	No	No	No	-6.73	0	0	0	0	0	0.55
9b	High	No	No	No	No	-6.55	0	0	0	0	0	0.55
9c	High	No	No	No	Yes	-6.49	0	0	0	0	0	0.55
9d	High	No	No	No	No	-6.85	0	0	0	0	0	0.55
9e	High	Yes	No	No	No	-6.61	0	0	0	0	0	0.55
9f	High	No	No	No	No	-7.09	0	0	0	0	0	0.55
9g	High	No	No	No	No	-6.52	0	0	0	0	0	0.55
9h	High	No	No	No	Yes	-6.28	0	0	0	0	0	0.55
9i	High	No	No	No	No	-6.75	0	0	0	0	0	0.55
9j	High	No	No	No	Yes	-6.52	0	0	0	0	0	0.55
9k	High	No	No	No	Yes	-6.29	0	0	0	0	0	0.55
9l	High	No	No	No	Yes	-6.76	0	0	0	0	0	0.55
9m	High	No	No	No	Yes	-6.19	0	0	0	0	0	0.55
9n	High	No	No	No	Yes	-5.95	0	0	0	0	0	0.55
9o	High	No	No	No	Yes	-6.42	0	0	0	0	0	0.55

Table 5. Computer aided ADME screening of the studied compounds:

Toxicity Prediction.

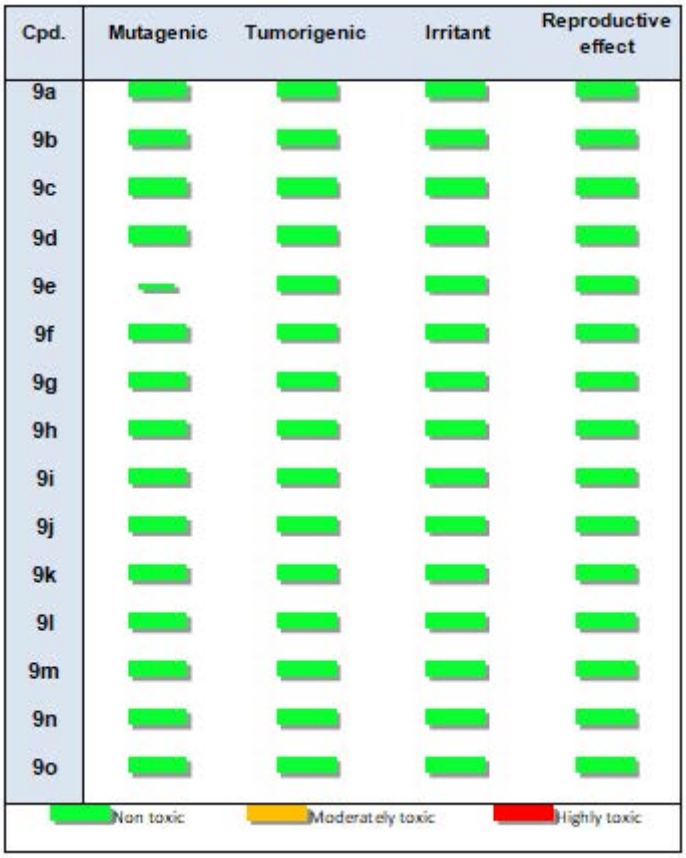

Figure 11. Orisis calculated toxicity risks of the studied compounds.

The final compounds 9a-o were additionally passed through one more web server; Osiris Property Explorer to assess their predicted toxicities. Prediction through this program is depending on the resemblance of the functional group of the examined compound with the *in vitro* and *in vivo* studied compounds comprised in its database. The output data are presented as color-coded; red, green, and yellow. Whereby, green color suggests low toxic potential, yellow proposes mild toxicity, and red color means high probability of toxicity [48,49]. The results presented that all the examined compounds are predicted to be safe showing no toxicity regarding tumorigenicity, mutagenicity, irritant effect, and effect on the reproductive system

Chemistry

Melting points (°C, uncorrected) were determined using a Stuart melting point apparatus. The IR spectra (KBr) were recorded on a SHIMADZU FT/IR spectrometer. The NMR spectra recorded by BRUKER 400 MHz NMR spectrometers use DMSO-d6 as solvent. Chemical shifts were reported in parts per million (δ), and coupling constants (J) expressed in Hertz. TMS was used as an internal standard and chemical shifts were measured in d ppm. 1H and 13C spectra were run at 400 and 100 MHz, respectively. Mass spectra were measured on an Agilent Triple Quadrupole 6410 QQQ LC/MS equipped with an ESI (electrospray ionization) source.

Synthesis of Enaminones 3a-e

To a solution of the appropriate ethenone 1a-e (20 mmol) in dry xylene (30 mL), dimethylformamide-dimethylacetal (2) (2.38 g, 20 mmol), was added and then the reaction was refluxed for 7 h. The solvent was distilled off and the product was triturated with diethyl ether (20 mL). The resulting solid was filtered and washed with cold petroleum ether to afford enaminones 3a-e, respectively. The physical properties of 3a-e were identical to those reported.

Synthesis of 3,4-dihydropyrimidin-2(1H)-Ones 9a-o

A mixture of the appropriate enaminone 3a-f (10 mmol), aldehyde 4a-c (10 mmol), and urea/thiourea (5a, b) (0.60 g, 10 mmol) in glacial acetic acid (25 mL) was refluxed for 6 h, then left to cool. The solid product filtered off, washed with ethanol, dried and finally recrystallized from EtOH/DMF to afford the corresponding 3,4-dihydropyrimidin-2(1H)-ones 9a-o, respectively.

5-Benzoyl-4-(Thiophen-2-yl)-3,4-Dihydropyrimidin-2(1H)-One (9a)

Pale yellow powder, 52% yield; mp 223-225°C; IR (KBr) νmax/cm^{-1} 3291, 3152 (2NH), 3034 (CH aromatic), 2259 (CH aliphatic), 1637, 1608 (2C=O); 1H NMR 5.71 (s, 1H, H-4 of pyrimidine), 6.83 (d, J=4.0 Hz 1H, Ar-H), 6.89-6.90 (m, 1H, Ar-H), 7.15 (d, J=4.0 Hz, 2H, Ar-H), 7.29 (d, J=4.0 Hz, 1H, Ar-H), 7.50 (s, D2O exchangeable, 1H, NH), 7.51-7.52 (m, 2H, 1H, Ar-H and H-6 of pyrimidine), 7.55-7.57 (m, 2H, 1H, Ar-H and H-6 of pyrimidine), 9.39 (s, D2O exchangeable, 1H, NH); 13C NMR δ49.81 (C-4 of pyrimidine), 116.19, 123.87, 124.58, 124.64, 125.51, 127.24, 127.37, 128.52, 128.86, 131.34, 139.64, 139.94, 151.08 (C=O of pyrimidine), 194.08 (C=O); MS *m/z:* 283 (M$^+$).

5-(4-Methylbenzoyl)-4-(Thiophen-2-yl)-3,4-Dihydropyrimidin-2(1H)-One (9b)

Pale yellow powder, 57% yield; mp 264-266°C; IR (KBr) νmax/cm-1 3239, 3144 (2NH), 3021 (CH aromatic), 2951 (CH aliphatic), 1654, 1652 (2C=O); 1H NMR 2.37 (s, 3H, CH3), 5.70 (s, 1H, H-4 of pyrimidine), 6.81 (s, 1H, Ar-H), 6.88 (s, 1H, Ar-H), 7.14 (s, 2H, Ar-H), 7.27-7.30 (m, 3H, 2H of Ar-Hs and 1H, D2O exchangeable, NH), 7.43 (s, 2H, 1H, Ar-H and H-6 of pyrimidine), 9.37 (s, D2O exchangeable, 1H, NH); 13C NMR δ 21.47 (CH3), 50.03 (C-4 of pyrimidine), 116.13, 123.79, 124.58, 127.20, 128.71, 129.36, 136.89, 139.46, 141.33, 151.24 (C=O of pyrimidine), 193.89 (C=O); MS *m/z*: 297 (M$^+$).

5-(4-CHLOROBENZOYL)-4-(thiophen-2-yl)-3,4-Dihydropyrimidin-2(1H)-One (9c)

Pale yellow powder, 55% yield; mp 236-238°C; IR (KBr) νmax/cm^{-1} 3235, 3158 (2NH), 3027 (CH aromatic), 2950 (CH aliphatic), 1665, 1607 (2C=O): 1H NMR 5.67 (s, 1H, H-4 of pyrimidine), 6.83 (s, 1H, Ar-H), 6.89 (s, 1H, Ar-H), 7.16 (s, 2H, Ar-H), 7.53-7.56 (m, 3H, 2H, Ar-H and 1H, D2O exchangeable, NH), 7.69 (s, 2H, 1H, Ar-H and H-6 of pyrimidine), 9.54 (s, D2O exchangeable, 1H, NH); 13C NMR δ 49.78 (C-4 of pyrimidine), 116.12, 123.98, 127.28, 128.99, 129.40, 130.44, 132.30, 135.32, 136.11, 138.27, 138.81, 140.08, 150.80 (C=O of pyrimidine), 192.86 (C=O); MS m/z: 318 (M$^+$).

5-(Furan-2-Carbonyl)-4-Phenyl-3,4 Dihydropyrimidin-2 (1H)-One (9d)

Brown powder, 70% yield; mp 202-204°C; IR (KBr) νmax/cm^{-1} 3242, 3115 (2NH), 3020 (CH aromatic), 2921 (CH aliphatic), 1708, 1651 (2C=O); 1H NMR 5.40 (s, 1H, H-4 of pyrimidine), 7.23-7.27 (m, 2H, Ar-H), 7.29-7.33 (m, 3H, Ar-H), 7.59 (s, 1H, H-6 of pyrimidine), 7.82 (s, 1H, Ar-H), 8.21 (s, 1H, Ar-H), 8.61 (s, 1H, Ar-H), 9.49 (s, D2O exchangeable, 1H, NH), 9.58 (s, D2O exchangeable, 1H, NH); 13C NMR δ 54.88 (C-4 of pyrimidine), 112.35, 113.62, 116.02, 117.31, 117.53, 122.59, 126.87, 127.87, 128.92, 140.43, 144.56, 146.57, 152.74 (C=O of pyrimidine), 191.39 (C=O); MS m/z: 267 (M$^+$).

4-(4-Chlorophenyl)-5-(Furan-2-Carbonyl)-3,4 Dihydropyrimidin -2 (1H)-One (9e)

Brown powder, 46% yield; mp 170-172°C; IR (KBr) νmax/cm^{-1} 3250, 3122 (2NH), 3040 (CH aromatic), 2921 (CH aliphatic), 1699, 1652 (2C=O); 1H NMR 5.39 (s, 1H, H-4 of pyrimidine), 7.31-7.33 (m, 2H, Ar-H), 7.39-7.42 (m, 2H, Ar-H), 7.59 (s, 1H, H-6 of pyrimidine), 7.84 (s, 1H, Ar-H), 8.21 (s, 1H, Ar-H), 8.60 (s, 1H, Ar-H), 9.78 (s, D2O exchangeable, 1H, NH), 10.61 (s, D2O exchangeable, 1H, NH); 13C NMR δ 54.58 (C-4 of pyrimidine), 117.43, 122.58, 128.40, 128.81, 130.05, 131.66, 137.87, 140.69, 143.50, 146.67, 149.68, 152.65 (C=O of pyrimidine), 192.60 (C=O); MS *m/z:* 301 (M$^+$).

5-(FURAN-2-Carbonyl)-4-(Thiophen-2-yl)-3,4-Dihydropyrimidin-2(1H)-One (9f)

Brown powder, 58% yield; mp 188-190oC; IR (KBr) νmax/cm^{-1} 3248, 3118 (2NH), 3015 (CH aromatic), 3270 (CH aliphatic), 1712, 1652 (2C=O); 1H NMR 5.60 (s, 1H, H-4 of pyrimidine), 6.81 (s, 1H, Ar-H), 7.29 (s, 1H, Ar-H), 7.60 (s, 1H, H-6 of pyrimidine), 7.69 (s, 1H, Ar-H), 7.98 (s, 1H, Ar-H), 8.20 (s, 1H, Ar-H), 8.62 (s, 1H, Ar-H), 9.81 (s, D2O exchangeable, 1H, NH), 10.63 (s, D2O exchangeable, 1H, NH); 13C NMR δ 49.58 (C-4 of pyrimidine), 112.44, 115.35, 117.53, 122.58, 124.61, 125.41, 126.99, 133.19, 138.15, 146.74, 152.68 (C=O of pyrimidine), 191.03 (C=O); MS *m/z:* 273 (M$^+$).

4-Phenyl-5-(Thiophene-2-Carbonyl)-3,4-Dihydropyrimidin-2(1H)-One (9g)

Yellow powder, 65% yield; mp 270-272oC; IR (KBr) νmax/cm-1 3270, 3093 (2NH), 3040 (CH aromatic), 2980 (CH aliphatic), 1674, 1645 (2C=O); 1H NMR 5.41 (s, 1H, H-4 of pyrimidine), 7.15-7.18 (m, 1H, Ar-H), 7.25-7.27 (m, 4H, Ar-H), 7.13-7.34 (m, 1H, Ar-H), 7.47-7.48 (m, D2O exchangeable, 1H, NH), 7.67 (s, 1H, H-6 of pyrimidine), 7.85 (s, 1H, Ar-H), 7.78-7.88 (m, 1H, Ar-H), 9.40 (s, D2O exchangeable,

1H, NH); 13C NMR δ 54.10 (C-4 of pyrimidine), 126.95, 127.93, 128.42, 128.96, 131.98, 132.70, 136.90, 140.38, 142.56, 143.88, 151.79 (C=O of pyrimidine), 186.34 (C=O); MS *m/z:* 283 (M^+).

4-(4-chlorophenyl)-5-(Thiophene-2-Carbonyl)-3,4-Dihydropyrimidin-2(1H)-One (9h)

Yellow powder, 60% yield; mp 246-248oCIR [51] (KBr) νmax/cm-1 3288-3050 (2NH+CH aromatic), 2913 (CH aliphatic), 1672, 1649 (2C=O); 1H NMR 5.41 (d, J=8.0 Hz, 1H, H-4 of pyrimidine), 7.15-7.19 (m, 1H, Ar-H), 7.31-7.35 (m, 2H, Ar-H), 7.38-7.42 (m, 2H, Ar-H), 7.47-7.51 (m, 1H, NH), 7.66-7.70 (m, 1H, C-6 of pyrimidine), 7.87-7.90 (m, 2H, Ar-H), 9.45 (d, J=8.0 Hz, D2O exchangeable, 1H, NH,); 13C NMR δ53.59 (C-4 of pyrimidine), 112.13, 128.43, 128.88, 129.57, 132.07, 132.96, 136.91, 137.10, 140.66, 142.93, 143.39, 151.64 (C=O of pyrimidine), 182.78 (C=O); MS *m/z*: 317 (M^+).

4-(Thiophen-2-yl)-5-(Thiophene-2-carbonyl)-3,4-Dihydropyrimidin-2(1H)-One (9i)

Yellow powder, 40% yield; mp 260-262oC; IR (KBr) νmax/cm-1 3408-3093 (2NH), 3040 (CH aromatic), 2955 (CH aliphatic), 1695-1589 (2C=O); 1H NMR 5.65 (s, 1H, H-4 of pyrimidine), 6.78 (s, 1H, Ar-H), 6.84 (s, 1H, Ar-H), 7.20-7.21 (m, 2H, Ar-H), 7.24 (s, D2O exchangeable, 1H, NH), 7.33-7.34 (m, 1H, H-6 of pyrimidine), 8.20 (s, 1H, Ar-H), 8.43 (s, 1H, Ar-H), 9.55 (s, D2O exchangeable, 1H, NH); 13C NMR δ50.94 (C-4 of pyrimidine), 115.73, 124.13, 127.09, 128.43, 129.72, 131.99, 132.85, 138.10, 142.55, 143.63, 150.78 (C=O of pyrimidine), 184.90 (C=O); MS *m/z*: 289 (M^+).

5-(Furan-2-Carbonyl)-4-Phenyl-2-Thioxo-1,2,3,4-Tetrahydropyrimidine (9j)

Brown powder, 48% yield; mp 240-242oC; 3266, 3177 (2NH), 3080 (CH aromatic), 2974 (CH aliphatic), 1640-1598 (C=S); 1H NMR 5.41 (s, 1H, H-4 of pyrimidine), 7.27-7.29 (m, 3H, Ar-H), 7.33-7.36 (m, 2H, Ar-H), 7.68 (s, 1H, H-6 of pyrimidine), 7.96 (s, 1H, Ar-H), 8.21 (s, 1H, Ar-H), 8.60 (s, 1H, Ar-H), 9.49 (s, D2O exchangeable, 1H, NH), 9.58 (s, D2O exchangeable, 1H, NH); 13C NMR δ 53.67 (C-4 of pyrimidine), 112.64, 113.12, 118.15, 122.58, 127.05, 129.10, 133.19, 137.87, 143.33, 147.24, 149.68, 151.51, 177.11 (C=S), 180.88 (C=O); MS *m/z*: 284 (M^+).

4-(4-chlorophenyl)-5-(furan-2-Carbonyl)-2-Thioxo-1,2,3,4-Tetrahydropyrimidine (9k)

Brown powder, 41% yield; mp 227-229oC; 3264-3117 (2NH), 3045 (CH aromatic), 2974 (CH aliphatic), 1651-1588 (C=O+C=S); 1H NMR 5.40 (s, 1H, H-4 of pyrimidine), 7.29-7.30 (m, 2H, Ar-H), 7.59-7.60 (m, 2H, Ar-H), 7.69 (s, 1H, H-6 of of pyrimidine), 7.96 (s, 1H, Ar-H), 8.21 (s, 1H, Ar-H), 8.60 (br s, 1H, Ar-H), 9.80 (s, D2O exchangeable, 1H, NH), 10.67 (s, D2O exchangeable, 1H, NH); 13C NMR δ53.10 (C-4 of pyrimidine), 112.66, 113.62, 118.25, 122.59, 128.98, 129.11, 130.51, 133.18, 137.87, 147.32, 149.69, 151.51, 177.00 (C=S), 180.39 (C=O); MS *m/z:* 318 (M^+).

5-(Furan-2-Carbonyl)-4-(Thiophen-2-yl)-2-Thioxo-1,2,3,4-Tetrahydropyrimidine (9l)

Brown powder, 55% yield; mp 175-177oC; 3268-3175 (2NH), 3020 (CH aromatic), 2950 (CH aliphatic), 1645-1595 (C=O+C=S); 1H NMR 5.65 (s, 1H, H-4 of pyrimidine), 6.85 (s, 1H, Ar-H), 7.27 (s, 1H, Ar-H), 7.59 (s, 1H, Ar-H), 7.66 (s, 1H, H-6 of pyrimidine), 7.99 (s, 1H, Ar-H), 8.21 (s, 1H, Ar-H), 8.60 (s, 1H, Ar-H), 9.91 (s, D2O exchangeable, 1H, NH), 10.73 (s, D2O exchangeable, 1H, NH); 13C NMR δ 48.74 (C-4 of pyrimidine), 112.71, 118.30, 122.59, 125.17, 127.39, 137.87, 146.79, 147.37, 149.69, 152.24, 176.73 (C=S), 180.57 (C=O); MS *m/z*: 289 (M^+).

4-Phenyl-5-(Thiophene-2-Carbonyl)-2-Thioxo-1,2,3,4-Tetrahydropyrimidine (9m)

Pale yellow powder, 45% yield; mp 255-257oC; 3183-3093 (2NH), 3072 (CH aromatic), 2962 (CH aliphatic), 1645-1618 (C=O+C=S); 1H NMR 5.42 (s, 1H, H-4 of pyrimidine), 7.19 (s, 1H, Ar-H), 7.28-7.30 (m, 1H, Ar-H), 7.31-7.34 (m, 3H, Ar-H), 7.73 (s, 1H, H-6 of pyrimidine), 7.91-7.93 (m, 2H, Ar-H), 8.43 (s, 1H, Ar-H), 9.76 (s, D2O exchangeable, 1H, NH), 10.54 (s, D2O exchangeable, 1H, NH); 13C NMR δ 54.19 (C-4 of pyrimidine), 113.43, 127.16, 128.34, 128.62, 129.58, 132.47, 133.57, 136.20, 138.62, 142.55, 142.70, 143.22, 174.34 (C=S), 183.10 (C=O); MS *m/z*: 300 (M^+).

4-(4-Chlorophenyl)-5-(Thiophene-2-Carbonyl)-2-Thioxo-1,2,3,4Tetrahydropyrimidine (9n)

Pale yellow powder, 63% yield; mp 208-210oC; 3440-3150 (2NH), 3077 (CH aromatic), 2988 (CH aliphatic), 1644-1619 (2C=O); 1H NMR 5.56 (s, 1H, H-4 of pyrimidine), 6.79-7.31 (m, 2H, Ar-H), 7.76 (s, 1H, H-6 of pyrimidine), 7.71-7.96 (m, 2H, Ar-H), 8.0-8.12 (m, 2H, Ar-H), 9.60 (s, D2O exchangeable, 1H, NH), 10.72 (s, D2O exchangeable, 1H, NH); 13C NMR δ 53.58 (C-4 of pyrimidine), 113.74, 115.48, 117.74, 122.73, 124.48, 125.84, 127.23, 134.42, 138.29, 146.03, 174.83 (C=S), 182.57 (C=O); MS *m/z*: 333 (M^+).

4-(Thiophen-2-yl)-5-(Thiophene-2-Carbonyl)-2-Thioxo-1,2,3,4-Tetrahydropyrimidine (9o)

Yellow powder, 43% yield; mp 260-262ºC; IR (KBr) νmax/cm^{-1} 3424-31120 (2NH), 3093 (CH aromatic), 2970 (CH aliphatic), 1645, 1636 (C=O+C=S); 1H NMR 5.66-5.68 (m, 1H, H-4 of pyrimidine), 6.97-7.02 (m, 2H, Ar-H), 7.21-7.24 (m, 1H, Ar-H), 7.31-7.34 (m, 1H, Ar-H), 7.43-7.46 (m, 1H, Ar-H), 7.74-7.76 (m, 1H, H-6 of pyrimidine), 7.91-7.98 (m, 1H, Ar-H), 9.90 (d, J=8.0 Hz, D2O exchangeable, 1H, NH), 10.66 (d, J=8.0 Hz, D2O exchangeable, 1H, NH); 13C NMR δ 49.19 (C-4 of pyrimidine), 113.65, 125.35, 126.32, 127.47, 128.69, 132.56, 133.70, 136.12, 142.47, 146.73, 174.63 (C=S), 182.76 (C=O); MS *m/z*: 305 (M^+).

Biological Screening

All biological screenings were performed at the Diagnostic and Confirmatory lab in the Holding Company for Biological Products and Vaccines (VACSERA), Giza, Egypt.

Anti-Proliferative Activity

The method defined was used for the evaluation of the anti-proliferative activity towards HCT-116, HeLa and MCF-7 cancer cell lines. The cell lines were gotten from American Type Culture Collection (ATCC, USA). Cells were cultured into 96-well microplates (cells density 1.2–1.8). 10,000 cells/well were used, and culturing was performed using Dulbecco's modified Eagle's medium (DMEM; Invitrogen/Life Technologies) supplemented with 10% FBS (Hyclone), 10 µg/ml of insulin (Sigma), and 1% penicillin-streptomycin at 37°C in a 5% CO_2 incubator. Cells then were incubated for 24 h at 37ºC in a humidified 5% CO_2 atmosphere.

Then the cells were exposed for 48 h to different concentrations of the compounds or doxorubicin. Then, the treated cells viability was determined via the MTT technique as follows: i) media were removed, ii) MTT solution (M-5655, Sigma Aldrich) was added, and incubated for an additional 4 h for metabolizing the dye to colored-insoluble formazan crystals. The remaining MTT solution was cast-off from the wells, and formazan crystals were solubilized. The plate was shaken at r.t. Absorbance was measured via a ROBONIK P2000 Elisa Reader at 570 nm. The cell viability was expressed as a concentration that exerts 50% of maximum inhibition of cell proliferation (IC_{50}) and it was determined *via* Graph Pad Prism version 5 software (Graph Pad software Inc, CA).

Cell Cycle Analysis

HCT-116, HeLa and MCF-7 cell lines were treated with the most potent compounds 9b, 9k and 9h, respectively at their IC_{50} concentrations for 48 h. After treatment, the cells were suspended in 0.5 mL of PBS, centrifuged for collection, and fixed in ice-cold ethanol (70% v/v), washed with PBS, resuspended with RNase, and stained with propidium iodide. Analysis was then performed by flow cytometry using FACScalibur (Becton Dickinson). Phoenix Flow Systems and Verity Software House were used for the calculation of the cell cycle distributions [50].

Apoptosis Assay

HCT-116, HeLa and MCF-7 cell lines were treated with the most potent compounds 9b, 9k and 9h, respectively at their IC_{50} concentrations for 48 h. After that, the cells were suspended in PBS, centrifuged, and fixed in ice-cold ethanol (70% v/v). Then, the ethanol suspended cells were centrifuged, suspended PBS, centrifuged again, and resuspended with PE Annexin V and PI staining solution according to the manufacturer's guidelines. At the end, analysis by flow cytometry using FACS Calibur (Becton Dickinson) was performed. Phoenix Flow Systems and Verity Software House were used for the cell cycle distributions calculations [51].

Cyclin Dependent Kinase 2/Cycline A2 Enzyme Inhibition

The *in vitro* CDK2/cyclin A2, and CDK9/cyclin T_1 enzyme inhibition assays were performed using the Promega Corporation CDK2 and the BPS Bioscience CDK9 luminescence kinase assay kits as described [53,53]. The assays were carried out at room temperature. The target compounds were dissolved and added to the reaction mixture at variant concentrations. Continuous kinetic monitoring of the enzyme activity was performed on Tecan–spark READER. The percent inhibition of the enzyme activity was calculated for all the compounds at four different concentrations, IC_{50} values were calculated via Graphpad prism, and each value represents the mean ± SD from triplicate determinants.

Molecular Modeling Study

Molecular docking study was performed using the Molecular Operating Environment (MOE 2014.0901) program. All minimization in docking procedures were achieved with MOE until RMSD gradient of 0.05 Kcal.mol-1 Å-1 with MMFF94 forcefield. Partial charges were automatically calculated. Triangle Matcher placement method and dG scoring function were utilized as a docking protocol. The X-ray crystal structures of the CDK2 enzyme co-crystallized with R-Roscovitine (PDB code: 3ddq) and CDK9 co-crystallized with the pyridine analogue AZD4573 (PDB code: 6z45) were downloaded from the protein data bank in PDB format and prepared for the docking study as follow.

For 3ddq protein

- Removal of chains C, D, E, water molecules and ligands that are not involved in the binding.
- Protonate 3D protocol with default options in MOE.

For 6z45 protein:

- Removal of chain A, water molecules and ligands that are not involved in the binding.
- Protonate 3D protocol with default options in MOE.

The studied compounds were built in 3D format using MOE and exposed to the following: i) structure 3D protonation. ii) Conformational analysis through systemic search. iii) Choosing the least energetic conformer. iv) Running the same docking protocol used with the native ligand.

In Silicon ADMET Study

SMILES notations of the studied compounds were nourished into the Swiss ADME web server to predict the pharmacokinetics and drug-likeness characteristics of the checked compounds. Another computational tool (Osiris Property Explorer was used to estimate of the possible toxicities like mutagenicity, tumorigenicity irritant and reproductive effect.

Conclusion

Novel series pyrimidines was synthesized, structurally elucidated, and evaluated for their anti-proliferative activity against human colorectal carcinoma HCT-116, cervical carcinoma HeLa and breast carcinoma MCF-7 cell lines. Compounds 9b, 9k and 9h were the most active ones against HCT-116, HeLa and MCF-7 cell lines (IC_{50}=2.46 ± 0.21, 1.81 ± 0.11 and 3.83 ± 0.27 µM, respectively) compared to doxorubicin (IC_{50}=2.39 ± 0.16, 3.02 ± 0.18 and 5.56 ± 0.3 µM, respectively). Potential anti-proliferative activity mechanisms were explored for the most potent compounds 9b, 9k and 9h. Cell cycle analysis showed that 9b, and 9k arrested the cell cycles of the treated HCT-116, and HeLa cells at G_1/S phase, while 9h arrested the MCF-7cell at G2-M phase. Also, compounds 9b, 9k and 9h are good apoptotic inducers within HCT-116, HeLa and MCF-7 cells, respectively. Moreover, compounds 9h and 9e dislayed promising CDK2 and CDK9 inhibitory acivities with IC_{50} values of 0.299 ± 0.02 and 0.396 ± 0.02, respectively. Molecular docking study showed similar binding modes of the studied compounds to that attained by the co-crystallized ligand either for CDK2 and or for CDK9 isoform. ADMET computational study predicted the good pharmacokinetic aspects for the studied compounds.

Acknowledgement

The authors acknowledge financial support from the Researchers Supporting Project number (RSP-2021/103), King Saud University, Riyadh, Saudi Arabia.

References

1. Shafei, Ayman, El-Bakly Wesam, Sobhy Ahmed, and Wagdy Omar et al. "A review on the efficacy and toxicity of different doxorubicin nanoparticles for targeted therapy in metastatic breast cancer." *Biomed Pharmacother.* 95 (2017): 1209-1218.
2. Decalf, Veerle H, MJ Huion Anja, F Benoit Dries, and Astrid Denys Marie, et al. "Older people's preferences for side effects associated with antimuscarinic treatments of overactive bladder: a discrete-choice experiment." *Drugs Aging*. 34 (2017): 615-623.
3. Wu, Qiong, Yang Zhiping, Nie Yongzhan, and Shi Yongquan, et al. "Multi-drug resistance in cancer chemotherapeutics: mechanisms and lab approaches." *Cancer let.* 347 (2014): 159-166.
4. Lin, Han-Syuan, Huang Yi-Luen, Stefanie Wang Yi-Rui, and Hsiao Eugene, et al. "Identification of novel anti-liver cancer small molecules with better therapeutic index than sorafenib via zebrafish drug screening platform." *Cancers* 11 (2019): 739.
5. V Iyer, Vidhya. "Small molecules for immunomodulation in cancer: a review." *Anti-Cancer Agents Med Chem* 15 (2015): 433-452.
6. Zhong, Zheng, Yu Jia, M Virshup David, and Madan Babita. "Wnts and the hallmarks of cancer." *Cancer and Metastasis Rev* 39 (2020): 625-645.
7. Laphanuwat, Phatthamon, and Jirawatnotai Siwanon. "Immunomodulatory roles of cell cycle regulators." *Front Cell Dev Biol* 7 (2019): 23.
8. Malumbres, Marcos, and Barbacid Mariano. "Cell cycle, CDKs and cancer: a changing paradigm." *Nat Rev Cancer* 9 (2009): 153-166.
9. Peyressatre, Marion, Prével Camille, Pellerano Morgan, and C Morris May. "Targeting cyclin-dependent kinases in human cancers: from small molecules to peptide inhibitors." *Cancers* 7 (2015): 179-237.
10. Manning, Gerard, B Whyte David, Martinez Ricardo, and Hunter Tony et al. "The protein kinase complement of the human genome." *Sci.* 298 (2002): 1912-1934.
11. Martin, Mathew P, A Endicott Jane, and EM Noble Martin. "Structure-based discovery of cyclin-dependent protein kinase inhibitors." *Essays Biochem* 61(2017): 439-452.
12. Asghar, Uzma, K Witkiewicz Agnieszka, C Turner Nicholas, and S Knudsen Erik. "The history and future of targeting cyclin-dependent kinases in cancer therapy." *Nat Rev Drug Discov* 14 (2015): 130-146.
13. Hu, Bing, Mitra Jayashree, van den Heuvel Sander, and H Enders Greg. "S and G_2 phase roles for Cdk2 revealed by inducible expression of a dominant-negative mutant in human cells." *Mol Cell Biol* 21 (2001): 2755-2766.
14. Donjerkovic, Dubravka, and W Scott David. "Regulation of the G1 phase of the mammalian cell cycle." *Cell res* 10 (2000): 1-16.
15. De Boer, Leonore, Oakes Vanessa, Beamish Heather, and Giles Nichole, et al. "Cyclin A/cdk2 coordinates centrosomal and nuclear mitotic events." *Oncogene* 27 (2008): 4261-4268.
16. Chung, Jon H, and Bunz Fred. "Cdk2 is required for p53-independent G2/M checkpoint control." *PLoS genet* 6 (2010): e1000863.
17. Rui Gao. "Design, synthesis, and optimisation of highly selective macrocyclic CDK9 inhibitors." *PhD diss* 2018.
18. Guardavaccaro, Daniele, and Pagano Michele. "Stabilizers and destabilizers controlling cell cycle oscillators." *Mol cell* 22 (2006): 1-4.
19. Siemeister, Gerhard, Lücking Ulrich, M Wengner Antje, and Lienau Philip, et al. "BAY 1000394, a novel cyclin-dependent kinase inhibitor, with potent antitumor activity in mono-and in combination treatment upon oral application." *Mol cancer ther* 11 (2012): 2265-2273.
20. Goh, K C, Diermayr V Novotny, Hart S, and Ong L C, et al. "TG02, a novel oral multi-kinase inhibitor of CDKs, JAK2 and FLT3 with potent anti-leukemic properties." *Leukemia* 26 (2012): 236-243.
21. Bettayeb, Karima, M Tirado Oscar, Marionneau Lambot Séverine, and Ferandin Yoan, et al. "Meriolins, a new class of cell death–inducing kinase inhibitors with enhanced selectivity for cyclin-dependent kinases." *Cancer Res* 67 (2007): 8325-8334.
22. Wang, Shudong, A Midgley Carol, Scaërou Frederic, and B Grabarek Joanna, et al. "Discovery of N-phenyl-4-(thiazol-5-yl) pyrimidin-2-amine aurora kinase inhibitors." *J Med Chem* 53 (2010): 4367-4378.
23. Heathcote, Dean A, Patel Hetal, HB Kroll Sebastian, and Hazel Pascale, et al. "A novel pyrazolo [1, 5-a] pyrimidine is a potent inhibitor of cyclin-dependent protein kinases 1, 2, and 9, which demonstrates antitumor effects in human tumor xenografts following oral administration." *J Med Chem* 53 (2010): 8508-8522.
24. Gregory, GP, Hogg SJ, Kats LM, and Vidacs E et al. "CDK9 inhibition by dinaciclib potently suppresses Mcl-1 to induce durable apoptotic responses in aggressive MYC-driven B-cell lymphoma in vivo." *Leukemia* 29 (2015): 1437-1441.
25. Martin, Mathew P, H Olesen Sanne, I Georg Gunda, and Schonbrunn Ernst. "Cyclin-dependent kinase inhibitor dinaciclib interacts with the acetyl-lysine recognition site of bromodomains." *ACS chem biol* 8 (2013): 2360-2365.
26. Hassan, Ghaneya S, E Abdel Rahman Doaa, M Nissan Yassin, and A Abdelmajeed Esraa, et al. "Novel pyrazolopyrimidines: Synthesis, in vitro cytotoxic activity and mechanistic investigation." *Eur J Med Chem* 138 (2017): 565-576.
27. Rosa, Fernanda A, Machado Pablo, G Bonacorso Helio, and Zanatta Nilo, and et al. "Reaction of β-dimethylaminovinyl ketones with hydroxylamine: A simple and useful method for synthesis of 3-and 5-substituted isoxazoles." *J Heterocycl Chem* 45 (2008): 879-885.
28. Kantevari, Srinivas, Venu Chary Mahankhali, and VN Vuppalapati Srinivasu. "A highly efficient regioselective one-pot synthesis of 2, 3, 6- trisubstituted pyridines and 2, 7, 7-trisubstituted tetrahydroquinolin-5-ones using K5CoW12O40· 3H2O as a heterogeneous recyclable catalyst." *Tetrahedron* 63 (2007): 13024-13031.
29. Darwish, Elham Sayed, Abdelshafy Abdelhamid Ismail, Adel Nasra Miead, and Abdel-Gallil Fathy Mohamed, et al. "A One-Pot Biginelli Synthesis of 6-Unsubstituted 5-Aroylpyrimidin-2 (1H)-ones and 6-Acetyl-1, 2, 4-triazin-3 (2H)-ones." *Helv Chim Acta* 93 (2010): 1204-1208.
30. Wan, Jie-Ping, and Jiang Pan Yuan. "Chemo-/regioselective synthesis of 6-unsubstituted dihydropyrimidinones, 1, 3-thiazines and chromones via novel variants of Biginelli reaction." *Chem commun* 19 (2009): 2768-2770.
31. Alinezhad, Heshmatollah, Mahmood Tajbakhsh, Zare Mahboobeh, and Mousavi Mahboobeh. "Phenylphosphinic acid-catalyzed synthesis of 6-unsubstituted dihydropyrimidinones under solvent-free conditions." *Heteroat Chem* 27 (2016): 290-294.
32. Alinezhad, Heshmatollah, Tajbakhsh Mahmood, Zare Mahboobeh, and Mousavi Mahbooeh. "Solvent-free synthesis of 6-unsubstituted dihydropyrimidinones using 2-pyrrolidonium bisulphate as efficient catalyst." *Chem Pap* 70 (2016): 1126-1130.
33. Mosmann, Tim. "Rapid colorimetric assay for cellular growth and survival: application to proliferation and cytotoxicity assays." *J Immunol Methods* 651-2 (1983): 55-63.
34. Pozarowski, Piotr, and Darzynkiewicz Zbigniew. "Analysis of cell cycle by flow cytometry." *J Immunol Methods* (2004): 301-311.
35. De Azevedo, Walter Filgueira, Leclerc Sophie, Meijer Laurent, and Havlicek Libor, et al. "Inhibition of cyclin-dependent kinases by purine analogues: crystal structure of human cdk2 complexed with roscovitine." *Eur J biochem* 243 (1997): 518-526.
36. Barlaam, Bernard, Casella Robert, Cidado Justin, and Cook Calum, et al. "Discovery of AZD4573, a potent and selective inhibitor of CDK9

that enables short duration of target engagement for the treatment of hematological malignancies." *J Med Chem* 63 (2020): 15564-15590.

37. Daina, Antoine, Michielin Olivier, and Zoete Vincent. "SwissADME: a free web tool to evaluate pharmacokinetics, drug-likeness and medicinal chemistry friendliness of small molecules." *Sci Rep* 7 (2017): 1-13.
38. Lipinski, Christopher A, Lombardo Franco, W Dominy Beryl, and J Feeney Paul. "Experimental and computational approaches to estimate solubility and permeability in drug discovery and development settings." *Adv Drug Deliv Rev* 23 (1997): 3-25.
39. Ghose, Arup K, N Viswanadhan Vellarkad, and J Wendoloski John. "A knowledge-based approach in designing combinatorial or medicinal chemistry libraries for drug discovery. 1. A qualitative and quantitative characterization of known drug databases." *J Comb Chem* 1 (1999): 55-68.
40. Veber, Daniel F, R Johnson Stephen, Cheng Hung-Yuan, and R Smith Brian, et al. "Molecular properties that influence the oral bioavailability of drug candidates." *J Med Chem* 45 (2002): 2615-2623.
41. Egan, William J, M Merz Kenneth, and J Baldwin John. "Prediction of drug absorption using multivariate statistics." *J Med Chem* 43 (2000): 3867-3877.
42. Muegge, Ingo, L Heald Sarah, and Brittelli David. "Simple selection criteria for drug-like chemical matter." *J Med Chem* 44 (2001): 1841-1846.
43. Campos, Mônica Caroline Oliveira, Barçante Castro-Pinto Denise, Alves Ribeiro Grazielle, and Moreira Berredo-Pinho Márcia, et al. "P-glycoprotein efflux pump plays an important role in Trypanosoma cruzi drug resistance." *Parasitol Res* 112 (2013): 2341-2351.
44. Lynch, Tom, and Price Neff Amy. "The effect of cytochrome P450 metabolism on drug response, interactions, and adverse effects." *Am Fam Physician* 76 (2007): 391-396.
45. Chang, Yen-Ching, Chen Chen-Peng, and Chen Chan-Cheng. "Predicting skin permeability of chemical substances using a quantitative structure-activity relationship." *Procedia Eng* 45(2012): 875-879.
46. Sander, T. "Actelion's property explorer." Allschwil, Switzerland: Actelion's Pharmaceuticals Ltd (2001).
47. Sander, Thomas, Freyss Joel, von Korff Modest, and Renée Reich Jacqueline, et al. "OSIRIS, an entirely in-house developed drug discovery informatics system." *J. Chem. Inf.* Model. 49 (2009): 232-246.
48. Nicoletti, I, Migliorati G, Pagliacci M C, and Grignani F, et al. "A rapid and simple method for measuring thymocyte apoptosis by propidium iodide staining and flow cytometry." *J Immunol Methods* 139 (1991): 271-279.
49. Vermes, István, Haanen Clemens, and Steffens-Nakken Helga, et al. "A novel assay for apoptosis flow cytometric detection of phosphatidylserine expression on early apoptotic cells using fluorescein labelled annexin V." *J Immunol Methods* 184 (1995): 39-51.
50. Abd El-Sattar, Nour EA, HK Badawy Eman, H AbdEl-Hady Wafaa, and IAbo-Alkasem Mohamed, et al. "Design and synthesis of new CDK2 inhibitors containing thiazolone and thiazolthione scafold with apoptotic activity." *Chem Pharm Bull* 69 (2021): 106-117.

How to cite this article: Sara T, Al-Rashood, Amal S Alharbi, and Hamad M Alkahtani. "Design, Synthesis and Anti-Proliferative Evaluation, CDK2/9 Inhibitory and Molecular Docking Studies of Certain New Substituted Pyrimidines ." *Med Chem* 12 (2022) : 610